Dynamic Compression of Rigid and Flexible Risers: Experimental and Numerical Results

Alexandre N. Simos
e-mail: alesimos@usp.br

André L. C. Fujarra
e-mail: afujarra@usp.br

Department of Naval Architecture and Ocean Engineering,
University of São Paulo,
São Paulo, SP, Brazil

Dynamic compression and buckling are critical issues in the viability analysis of rigid and flexible risers developed for offshore applications, especially concerning deep-water operations. Those subjects have been addressed both numerically and analytically. However, few experimental data for validation purposes is found in literature. This paper presents a set of experimental results on the dynamic compression of rigid and flexible risers in catenary configurations, obtained by means of towing-tank tests. Two small-scale models have been built, the first one emulating the dynamic behavior of a steel catenary riser (SCR) and the other representing a much more flexible line. Uniform circular motion has been applied to the top of the models, emulating the floating system first-order oscillations. Different amplitudes of top motion have been considered, each one of them imposed with different frequencies of oscillation. Tension has been measured at the top of the models. The influence of current velocity has also been evaluated. Dynamic tension estimations obtained through finite element analysis are compared to the experimental results. Tension amplitude and critical compression load values are evaluated and compared for both, the steel catenary (SCR) and the flexible models. Comparisons show, in general, a fair agreement between simulations and experiments, reassuring the reliability of numerical models. Results also demonstrate that finite element code provides good predictions of maximum tension loads even when the risers are subjected to high levels of dynamic compression and buckle. Nevertheless, it is clearly noted that difficulties arise in the treatment of flexible structures under severe buckling and torsion. The accuracy of analytical methods proposed for the estimation of critical compression loads is also discussed, based on the experimental results.
[DOI: 10.1115/1.2199560]

Keywords: risers, catenary configuration, dynamic compression, towing-tank tests, fem method, buckling loads

Introduction

As offshore production systems move to deeper waters, riser design becomes a more and more critical issue, both from technical and economical points of view. Unquestionably, achieving a reasonable level of confidence on the design of such structures is not an easy task. Difficulties arise from many aspects as, for example, the uncertainties regarding environmental excitation and soil interaction.

One of the critical subjects involving riser design and its structural analysis is the *dynamic compression* phenomenon. Dynamic compression occurs on a specific section of the line when the time-varying component of the tension, the so-called *dynamic tension*, surpasses the static tension component on that section, what may lead to buckling of portions of the riser. Although deep-water risers behave almost like cables [1], their nonzero bending stiffness (EJ) provide some resistance to buckling and, therefore, risers can support a certain level of compression. The critical compression load refers to the minimum load magnitude that results in buckling of the structure and its value depends on the curvature and also on the eventual torsion of the line. When attached to floating systems that may present significant wave-induced motions as, for example, FPSO systems, determining an allowable level of dynamic compression on the risers is crucial to assess their viability.

For design purposes, the problem of predicting the dynamic tension along a particular submerged line is usually addressed numerically. Solution provided by numerical methods as, for example, finite element methods (FEM), is relatively straightforward for this kind of application, although dealing with dynamically compressed risers generally requires smaller elements and, therefore, higher computational effort.

Analytical approach for estimating the dynamic tension and critical load on risers also present good results and it is certainly more suitable for early stages of design, when several parameters have to be adjusted and a broad set of analysis has to be performed. Aranha and Pinto [2] presented an algebraic approximation for the dynamic tension on risers and mooring lines. Aranha et al. [3] provided an analytic approximation for the critical load on risers, which agreed very well with numerical results, both for steel catenary risers and flexible risers analysis. Ramos, Jr. and Pesce [4] later extended the approximation to the more general case of compression coupled with twisting of the line.

The main goal of this work is to provide some experimental results on dynamic compression of rigid and flexible lines and to address a preliminary comparison with numerical results. The main purpose of this analysis is to compare the dynamic tension results obtained experimentally with numerical predictions generated by means of FEM time-domain simulations and also to evaluate the accuracy of analytical methods developed for the estimation of critical compression loads. As noticed by Aranha and Pinto [2], although numerical analysis of dynamically compressed risers can be done in a relatively straightforward manner, it is not unusual that different numerical codes provide distinct predictions of dynamic tension. Analytical formulations, on the other hand, de-

Contributed by the Ocean Offshore and Arctic Engineering Division of ASME for publication in the JOURNAL OF OFFSHORE MECHANICS AND ARCTIC ENGINEERING. Manuscript received August 25, 2004; final manuscript received July 27, 2005. Assoc. Editor: Ron Riggs.

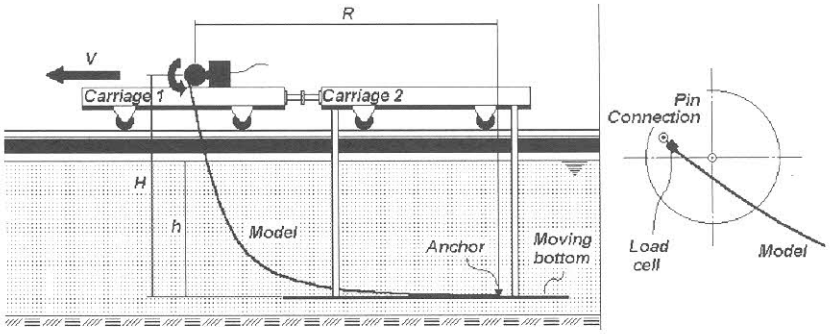

Fig. 1 Sketch of the experimental setup at IPT

pend on the hypothesis that riser dynamics remains confined to the plane defined by its catenary. This is not always accurate, especially for dynamically compressed flexible risers. Nevertheless, it is important to emphasize that there is no intention to provide an exhaustive comparison between experimental and theoretical results. On the contrary, the experimental results obtained with the two small-scale riser models with very different bending stiffness are used here to point out some important aspects concerning riser dynamics and the dynamic compression phenomenon.

In the first part of the paper, the experimental setup and the small-scale models are described. The experimental results obtained in the towing-tank are fully presented. Later on, dynamic tension amplitudes and critical loads obtained in the tests are compared to the predictions provided by the software ORCAFLEX® [5]. Also, bearing in mind that an appropriate estimation of the allowable compression loads on risers is nowadays one of the most important parameters in deep-water riser design, critical compression load values derived from experimental measurements are compared to the analytical predictions proposed by Aranha et al. [3] as well as with numerical predictions.

Experimental Setup

Tests were conducted at the State of São Paulo Technological Research Institute (IPT) towing tank, 240 m long, 6 m wide, and 4 m deep. Since the small-scale models had to be carried along the tank to emulate current effects, a moving bottom was built for these tests. The moving bottom was connected to the carriage and supported the models anchors. Harmonic circular motions with different combinations of amplitude and frequency were imposed to the top of the models by means of a rotating device mounted on the carriage. Load cells mounted on the top of each model measured the time-varying tension on the lines. Load cells were attached to the rotating mechanism by means of a pin connection, therefore, the tops of the models were free to rotate. Figure 1 presents a sketch of the experimental setup. Data acquisition was performed by means of a standard A.D. device with sampling frequency high enough to avoid aliasing problems.

Tests were performed with null velocity and also with $V = \pm 0.2$ m/s, the positive sign representing a top-to-anchor current velocity. The current profiles emulated were, therefore, uniform along the depth with velocity vectors parallel to the plane of the catenary.

Small-Scale Rigid Model. The dynamics of a rigid riser (SCR) was emulated by means of a small-scale model, which consisted of an 8.85 m long steel wire rope with a diameter of 3.5 mm. Main features of the model are specified in Table 1, which also presents the excitation parameters applied in the tests.

Where:

D_{ext}	External diameter
L_T	Total length of the model
h	Water depth
R	Horizontal distance anchor-top
H	Vertical distance anchor-top
EA_{eq}	Equivalent axial stiffness
EJ_{eq}	Equivalent bending stiffness
q	Weight per unit of length, in air
θ_{TOP}	Angle on the top (neutral position)
V	Current velocity
A	Amplitude of the motion (circular)
F	Imposed frequency

Small-Scale Flexible Model. A much more flexible riser was represented by means of a model consisting of a steel strip (10.0 mm × 1.0 mm, the 10.0 mm side being normal to the plane of the riser), covered by a circular external rubber layer, providing a 12 mm external diameter (see Fig. 2). The external rubber coat was applied for hydrodynamic purposes only, since the model bending stiffness depended almost exclusively on the steel strip. Discrete weights were regularly distributed along the model in order to increase its total weight per unit of length (q), providing a value of $q = 2.193$ N/m (in air).

For the ballasted model the angle at the top of the line resulted approximately 48 deg with respect to the horizontal plane. It might be argued that this value is somewhat low compared to those usually observed for real deep-water risers. Nevertheless, it must be kept in mind that the main purpose of the tests was to provide experimental results for validation of numerical and analytical models, rather than reproducing real riser configurations. The main particulars of the flexible model and the experimental parameters used in the tests are presented in Table 2.

Table 1 Main parameters of the experimental setup. Rigid model.

D_{ext} (mm)	3.50
L_T (m)	8.85
h (m)	3.0
R (m)	7.20
H (m)	3.36
EA_{eq} (kN)	2020.4
EJ_{eq} (kN·m^2)	1.5469×10^{-3}
q (N/m)	0.736
θ_{TOP} (deg)	71
V (m/s)	0, ±0.20
A (m)	0.075, 0.100, 0.150
F (Hz)	0.750, 1.000, 1.125, 1.500

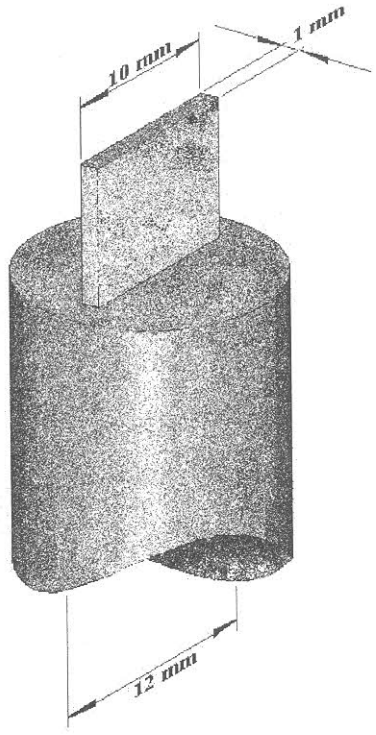

Fig. 2 Layout of the flexible small-scale model

Compilation of the Experimental Results

Experimental Results for the Rigid Model. Figure 3 presents an excerpt of a typical time-series of the tension (T) measured at the suspended end of the rigid model. For most tests, dynamic compression was achieved even at the top of the model. Tension amplitude remained relatively constant in time. Although submitted to high-levels of dynamic compression, no out-of-plane oscillations or buckling of the model were observed in the tests.

The whole set of experimental results obtained for the rigid model without current effects ($V=0$) is summarized later, in Fig. 4, together with numerical results, which will be discussed ahead in the paper. Results in Fig. 4 present the maximum tension obtained in each test (T_{max}) normalized by the static tension at the top of the model (T_0). For the zero current condition, $T_0 = 2.96$ N. It can be seen that, for the three different amplitudes of motion imposed to the top, experimental values of tension increase monotonically with respect to the frequency of oscillation, as predicted by numerical and analytical studies.

Current effects on the model dynamics may be inferred through Figs. 5 and 6, which present the normalized maximum tension

Table 2 Main parameters of the experimental setup. Flexible model case.

D_{ext} (mm)	12.0
L_T (m)	8.0
h (m)	3.0
R (m)	7.0
H (m)	3.36
EA_{eq} (kN)	265.25
EJ_{eq} (kN·m^2)	2.6384×10^{-4}
q (N/m)	2.193
θ_{TOP} (deg)	47.8
V (m/s)	0, ±0.20
A (m)	0.050, 0.075, 0.100, 0.150
F (Hz)	0.750, 1.000, 1.250, 1.500

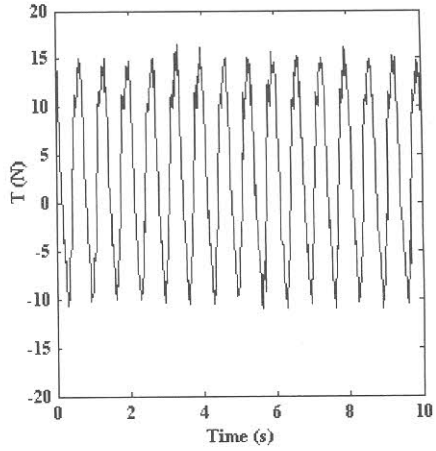

Fig. 3 Time-series of the top tension on the rigid model. $A = 150$ mm, $F = 1.52$ Hz, $V = 0$.

(T_{max}/T_0) obtained in the tests with $V = +0.2$ m/s and $V = -0.2$ m/s, respectively. Experimental values of static tension at the top corresponded to $T_0 = 2.72$ N for positive velocity and $T_0 = 3.50$ N for negative velocity.

It should be noted that, compared to the zero current results, current effects were pronounced only for the highest amplitude of top motion ($A = 0.150$ m). For smaller amplitudes of excitation, current effects resulted almost negligible for the velocities adopted in the tests.

Experimental Results for the Flexible Model. A typical tension signal measured at the suspended end of the flexible model is presented in Fig. 7. In contrast with the rigid model results, very irregular tension amplitudes were observed along the tests, especially for the higher amplitudes of top motion. Such irregular behavior is related to buckling and torsion of the line and consequent out-of-plane oscillations of the model, which could be observed along the tests.

For high amplitudes of top motion, as is the case in Fig. 7 ($A = 0.150$ m), it can be clearly observed that the compression loads reach a limit value, corresponding to the buckling load at the top of the model. This limit value of compression will be named *critical compression load*. In the tests corresponding to the most severe loading cases (high amplitudes and frequencies of oscillation), buckling of the model could indeed be visually inferred in

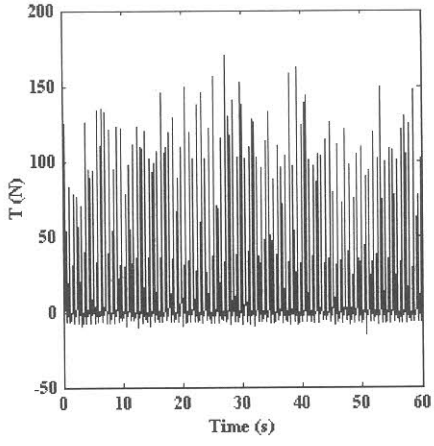

Fig. 4 Normalized maximum tension results. Rigid model. $V = 0$. Experimental: (▲) $A = 150$ mm, (■) $A = 100$ mm, (♦) $A = 75$ mm. Numerical: (△) $A = 150$ mm, (□) $A = 100$ mm, (◇) $A = 75$ mm.

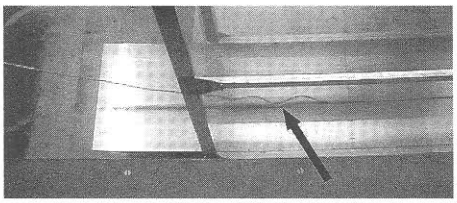

Fig. 5 Normalized maximum tension results. Rigid model. V = +0.2 m/s. Experimental: (▲) A=150 mm, (■) A=100 mm, (♦) A=75 mm. Numerical: (△) A=150 mm, (□) A=100 mm, (◇) A =75 mm.

the form of a *wave* that propagated along the model, from the *touchdown* region towards the top (see Fig. 8).

Normalized maximum tension results for the flexible model in zero current condition are presented later, in Fig. 9, which summarizes the results obtained for all the different combinations of amplitude and frequency of excitation. The measured static tension in this case corresponded to T_0=11.82 N.

Experimental results in Fig. 9 demonstrate that, as the amplitude of top motion increases, tension amplitude presents a different behavior regarding its variation with the frequency of excitation. For A=0.050 m, a monotonic increase of the tension amplitude with frequency is obtained. For higher values of amplitude, on the other hand, a different trend is observed and the rate of increase of tension amplitude decays for higher frequencies of excitation.[1] Once again, this behavior is related to buckling and out-of-plane oscillations of the model.

The same trend is verified under current action, as shown in Figs. 10 and 11, respectively, for V=+0.2 m/s (T_0=9.93 N) and V=−0.2 m/s (T_0=13.74 N). In fact, results indicate that the current effects are now more pronounced and play an important role in the dynamics of the flexible model.

Numerical Analysis of Rigid Model Results

In this section, dynamic tension amplitudes measured at the suspended end of the SCR riser model are compared to the results provided by the software ORCAFLEX® [5]. ORCAFLEX® is a validated commercial package, which presents a three-dimensional (3D) nonlinear time-domain finite element program for the dynamic analysis of risers and mooring systems. Line modeling is done by means of a lumped mass model and assumes axisymmetric mechanical properties of the line.

Figure 12 provides a comparison between the experimental time-series of tension measured at the top of the SCR model and the one predicted numerically for one of the tests with the highest amplitude of top motion (A=0.150 m and F=1.00 Hz).

It can be inferred from Fig. 12 that, even for the highest values of amplitude and frequency of top motion, the tension response is nearly harmonic. The numerical model reproduces maximum tension very well. There is no evidence that a critical compression load was reached at the top of the model. No out-of-plane oscillations were observed during the tests or in time-domain simulations. Analysis of tension signals demonstrates that almost all the energy of the signal is concentrated in a very narrow band around the frequency of excitation. This can be inferred in Fig. 13, which brings the power spectra of the tension signals presented in Fig. 12.

Comparisons of normalized maximum tension (T_{max}/T_0) derived from the towing-tank tests and numerical predictions are condensed in Figs. 4–6. They present the tension results for the three different current conditions considered in the tests, V=0

[1]It should be noticed that a similar behavior was observed by Aranha and Pinto [2] for the tension amplitude at the TDP of a steel catenary riser, predicted by means of numerical time-domain simulations performed with two different codes.

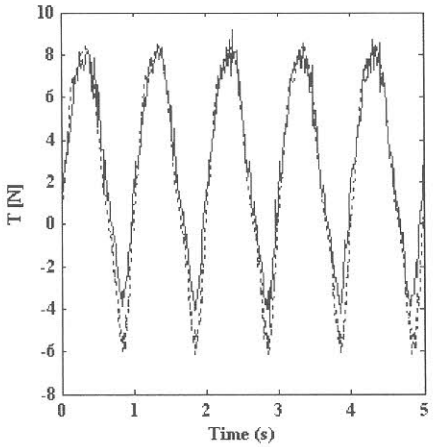

Fig. 6 Normalized maximum tension results. Rigid model. V =−0.2 m/s. Experimental: (▲) A=150 mm, (■) A=100 mm, (♦) A=75 mm. Numerical: (△) A=150 mm, (□) A=100 mm, (◇) A =75 mm.

(T_0=2.96 N), V=+0.2 m/s (T_0=2.72 N) and V=−0.2 m/s (T_0 =3.50 N), respectively. A seventy elements mesh was adopted for numerical simulations, the size of the mesh being chosen after convergence analysis.

The mechanical properties of the model adopted for simulations correspond to those obtained experimentally, already presented in Table 1. Time-step for calculations were kept under 1/20th of the shortest natural period of the model. The shortest natural period,

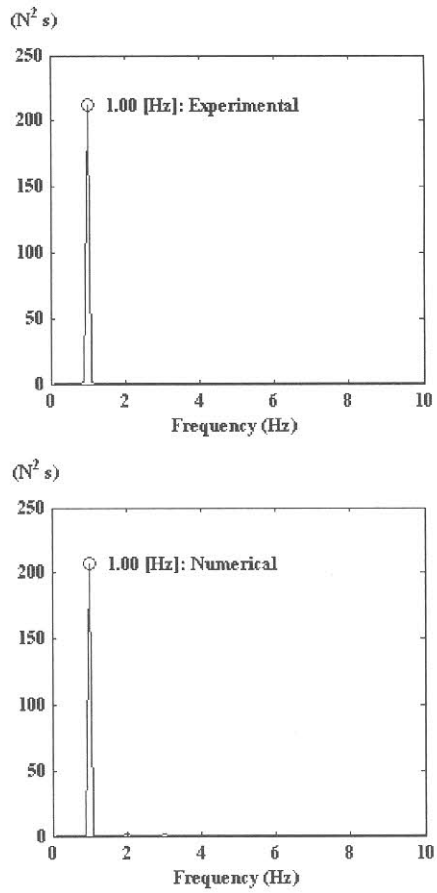

Fig. 7 Time-series of the top tension on the flexible model. A =150 mm, F=1.50 Hz, V=0.

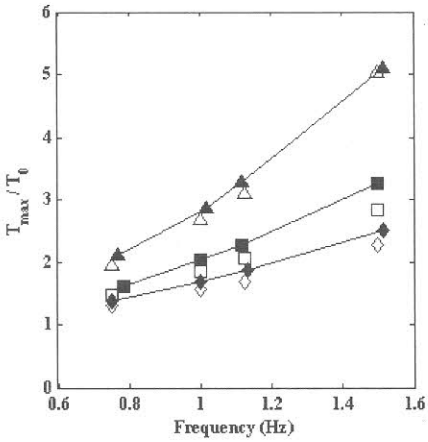

Fig. 8 Propagating wave arising from buckling at the TDP region of the flexible model

in this case, corresponded to 86×10^{-6} s. All simulations were performed for a minimum of 50 cycles of oscillations to guarantee steady-state response.

Comparisons show a very good agreement between experimental and numerical results. The FEM code is able to reproduce the model dynamics well, even for the most extreme case of dynamic compression. It should be noted that the dynamic tension amplitude was up to five times the static tension at the top of the model.

Numerical Analysis of Flexible Model Results

It was already pointed out that the tests performed with the flexible model provided a much richer dynamic behavior. Critical compression loads were reached even at the top of the model and the dynamics involved torsion, buckling and out-of-plane oscillations.

Figure 14 presents a comparison of the time-series of tension measured in a test with $A=0.100$ m and $F=1.00$ Hz and the corresponding numerical prediction.

The comparison presented in Fig. 14 illustrates the overall agreement obtained for smaller amplitudes and frequencies of top motion, but the same level of accuracy was not observed for the whole set of experimental conditions. As the amplitude and frequency increases, the model undergoes severe buckling even at the top, leading to out-of plane oscillations and, as a consequence, the tension fluctuation in time was more pronounced. In fact, the

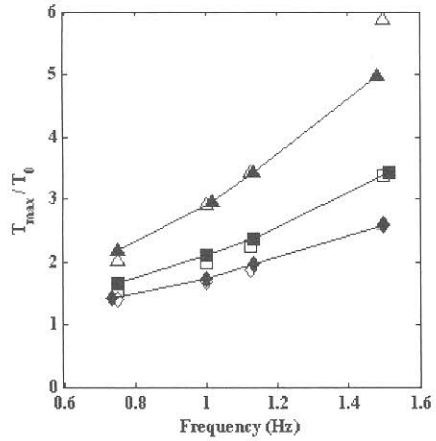

Fig. 9 Normalized maximum tension results. Flexible model. V=0. Experimental: (▲) A=150 mm, (■) A=100 mm, (♦) A =75 mm, and (×) A=50 mm. Numerical: (△) A=150 mm, (□) A=100 mm, (◇) A=75 mm, and (+) A=50 mm.

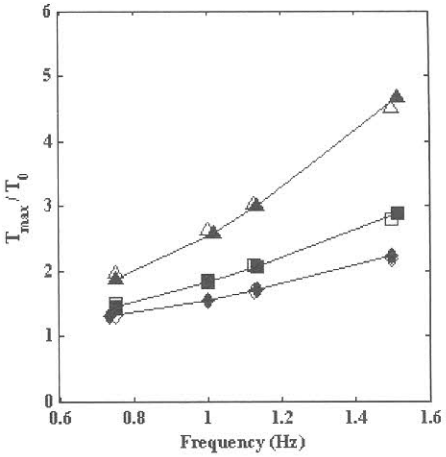

Fig. 10 Normalized maximum tension results. Flexible model. V=+0.2 m/s. Experimental: (▲) A=150 mm, (■) A=100 mm, (♦) A=75 mm, and (×) A=50 mm. Numerical: (△) A=150 mm, (□) A=100 mm, (◇) A=75 mm, and (+) A=50 mm.

analysis of experimental tension signals demonstrates the contribution of several higher harmonics. Figure 15 presents a comparison of the power-spectra derived from the signals in Fig. 14.

The experimental power-spectrum demonstrates that the test results presented significant contributions of several sub-harmonics. Furthermore, it must be reminded that the small-scale riser model configuration was based on a steel strip and, therefore, presented different bending stiffness for in-plane and out-of-plane oscillations, a feature that could not be represented by the numerical code, since axisymmetric bending is assumed in the numerical model. This configuration might be responsible for the discrepancies observed, since torsion will not occur in the same way.

The agreement for normalized maximum tension (T_{max}/T_0) concerning the flexible model analysis can be inferred from Figs. 9–11, which present the comparison between experimental and numerical results for the three different current conditions, V=0 (T_0=11.82 N), V=+0.2 m/s (T_0=9.93 N) and V=−0.2 m/s (T_0 =13.74 N), respectively.

Once again, convergence analysis demonstrated that a seventy elements mesh was sufficient for numerical simulations, concerning the stabilization of maximum tension amplitudes. However, transitory response was now much more pronounced and some-

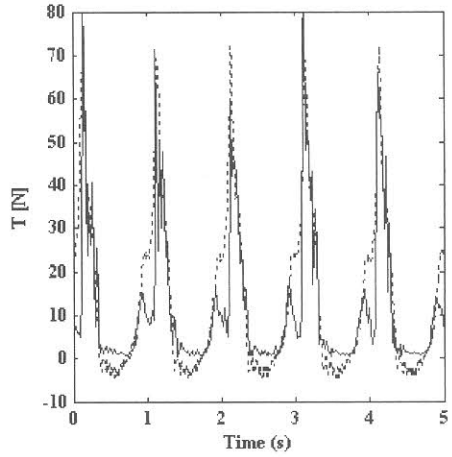

Fig. 11 Normalized maximum tension results. Flexible model. V=−0.2 m/s. Experimental: (▲) A=150 mm, (■) A=100 mm, (♦) A=75 mm, and (×) A=50 mm. Numerical: (△) A=150 mm, (□) A=100 mm, (◇) A=75 mm, and (+) A=50 mm.

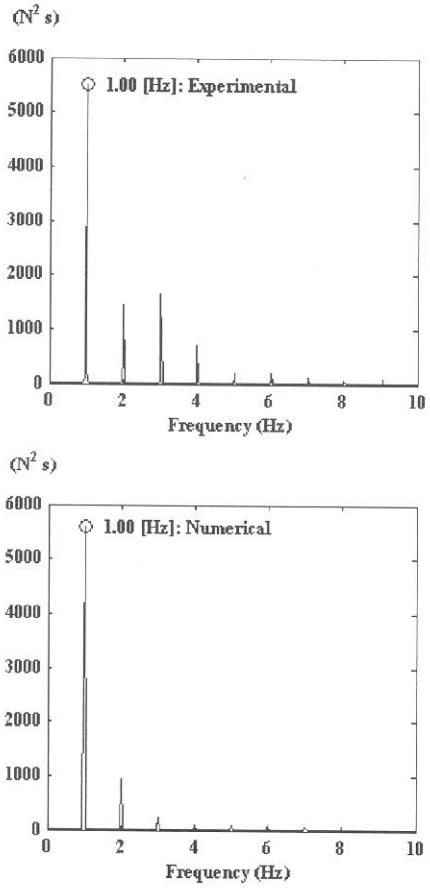

Fig. 12 Excerpt of time-series of tension at the top of rigid model. A=150 mm, F=1.00 Hz; V=0. (—numerical; —experimental).

times required the simulation of 100 cycles in order to guarantee steady-state response. As a rule, the total time of simulation required increased with amplitude and frequency and was connected to the beginning of out-of-plane response. The time-step was 10×10^{-6} s.

Compared to the results obtained for the rigid model, it can be readily seen that the agreement between numerical and experimental results is now much more difficult. As could be anticipated, discrepancies grow with the level of dynamic compression and buckling, which are more significant for $V=+0.2$ m/s (as a result of the lower static tension). The tests indicated that buckling of the model was followed by intense out-of-plane oscillations, which were certainly enlarged due to the structural configuration of the model (the use of a steel strip). As previously mentioned, the non-axisymmetric bending properties of the structure could not be modeled in the numerical code and, therefore, the torsion of the line could not be correctly reproduced. This is certainly one of the reasons for the discrepancies. Nonetheless, it is noteworthy that results in Fig. 11 ($V=-0.2$ m/s) indicate that as soon as the level of buckling is reduced (due to an increase in static tension), numerical predictions once again get closer to the experimental values. This is indeed an outstanding result since, even for $V=-0.2$ m/s, the model was subjected to high levels of dynamic compression and buckling.

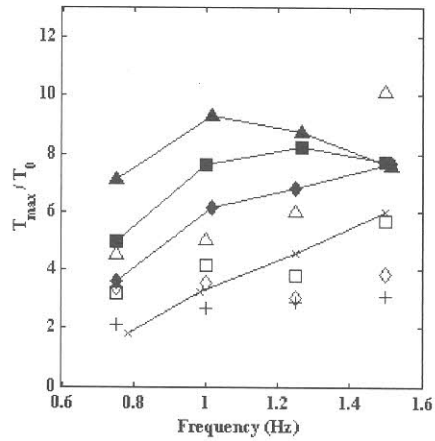

Fig. 14 Excerpt of time-series of tension at the top of flexible model. A=100 mm, F=1.00 Hz; V=0 (--- numerical; — experimental).

The Critical Compression Load

The maximum value of compression allowable for a particular deep-water riser is one of the most important parameters involved in its design. Therefore, some aspects of the experimental results here presented deserve special attention.

Aranha et al. [3] proposed a very simple analytical formulation for the estimation of the quasi-steady buckling load of a curved riser, named *critical load*. The critical load therefore corresponds to the maximum compression load that would be measured on a particular segment of the riser that undergoes buckling. The analytical model takes into account the effect of beam curvature in

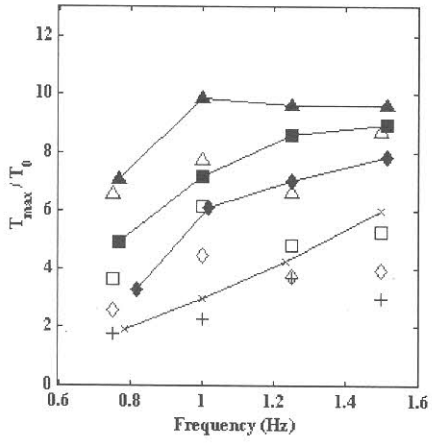

Fig. 13 Power Spectra of tension at the top of the rigid model. A=150 mm, F=1.00 Hz; V=0.

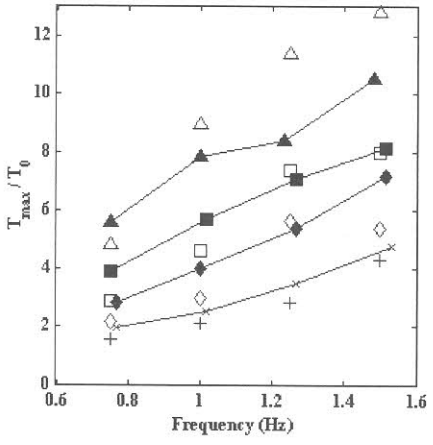

Fig. 15 Power spectra of tension at the top of flexible model. A=0.100 m, F=1.00 Hz; V=0.

Table 3 Analytical predictions of critical load at the top of rigid model

F (Hz)	P_{cr}/T_0
0.75	4.84
1.00	6.45
1.13	7.25
1.50	9.67

the calculations of buckling loads. The value of compression that leads to buckling is called P_{cr} and its value depends on the particular position of the line under analysis since static tension and curvature vary along the riser.

If χ denotes the curvature of the riser, m is the mass per unit length, m_a is the added mass per unit length and EJ is the bending stiffness, Aranha et al. [3] propose the following expression for the calculation of the local buckling load:

$$P_{cr}(\chi) = 2\pi F \beta_{cr}^2(\chi)\sqrt{(m+m_a)EJ} \quad (1)$$

The parameter β_{cr} is obtained as the solution of an eigenvalue problem of the curved beam.

According to the formulation presented in [3], for the SCR model the maximum compression loads at the top of the model were below the critical values for the whole set of conditions tested. For example, for the tests with $V=0$, the values of predicted critical load at the top of the model range from $P_{cr}=14.32$ N for $F=0.75$ Hz to $P_{cr}=28.63$ N for $F=1.50$ Hz. Indeed, experimental results show no indication of buckling since a limit compression value was never observed in the time-series. Table 3 presents the theoretical values of the critical load, calculated according to (1), normalized by the static tension at the top. The solution of the eigenvalue problem indicates that for the rigid model $\beta_{cr}=2.984$ for all frequencies.

Figure 16 presents the values of minimum tension (T_{min}) measured in each one of the tests conducted with the rigid model, as a function of the top motion amplitude. Once again, values are normalized by the static tension. Negative values of T_{min}/T_0 indicate compression. Results in Fig. 16 confirm that critical compression loads have not been reached in the tests with the rigid model.

In order to provide a quantitative comparison with the analytical predictions, some higher values of amplitude (A) were simulated numerically until a saturation of compression loads could be observed. Figure 17 presents the experimental and numerical results of T_{min}/T_0 for the frequencies $F=0.75$ Hz and $F=1.50$ Hz, including the numerical values obtained for higher amplitudes. For the sake of comparison, the analytical predictions of P_{cr}/T_0 at

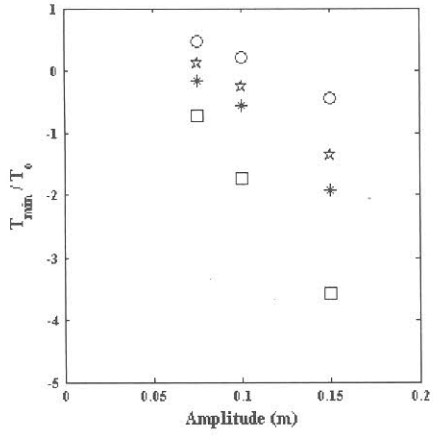

Fig. 16 Experimental values of normalized minimum tension loads. Rigid Model. $V=0$. (○) $F=0.75$ Hz, (☆) $F=1.00$ Hz, (*) $F=1.125$ Hz and (□) $F=1.50$ Hz.

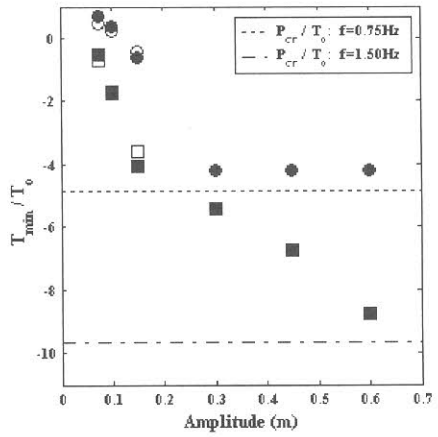

Fig. 17 Normalized minimum tension loads. Rigid model. $V=0$. Experimental: (○) $F=0.75$ Hz and (□) $F=1.50$ Hz. Extended numerical results: (●) $F=0.75$ Hz and (■) $F=1.50$ Hz.

the top of the model are represented by the dashed horizontal lines ($P_{cr}/T_0=4.84$ for $F=0.75$ Hz and $P_{cr}/T_0=9.67$ for $F=1.50$ Hz).

Figure 17 demonstrates that the numerical model reproduces very well the minimum tension values observed in the experiments. For $F=0.75$ Hz, numerical results indicate a critical compression value that agrees very well with the analytical predictions. Also, for $F=1.50$ Hz, results confirm that the critical load has not been reached even for $A=0.60$ m, attesting that the variation of P_{cr} with the frequency of oscillation is indeed well captured by Eq. (1).

Finally, Fig. 18 presents an excerpt of the time-series of nondimensional tension (T/T_0) obtained numerically for $A=0.60$ m, $F=0.75$ Hz, and $V=0$. The saturation of compression close to the critical value of P_{cr}/T_0 can already be visualized, once again demonstrating the good agreement between numerical and analytical predictions of the buckling load.

For the flexible model, on the other hand, experimental results indicate that critical compression loads on the top were reached in several tests. However, comparison of analytical and experimental results in this case cannot be provided since the analytical formulation is strictly two-dimensional [6]. Buckling of the flexible model was always followed by significant out-of-plane oscillations. The structural configuration of the model, with nonaxisymmetric bending stiffness contributed to this behavior. Experimental results demonstrated that the critical loads were very small, with buckling occurring as soon as the line started to be dynami-

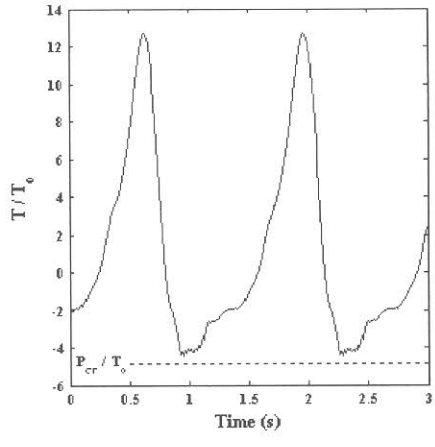

Fig. 18 Excerpt of normalized tension series. Rigid model. $A=0.60$ m; $F=0.75$ Hz; $V=0$.

cally compressed, regardless the frequency of excitation. Application of the two-dimensional analytical formula (1), in this case, leads to P_{cr} values that are overestimated, as could be anticipated.

Finally, it must be emphasized that, despite the differences observed for the maximum tension loads of the flexible model, the numerical FEM code was always able to reproduce the correct values of buckling loads.

Conclusions

Tension amplitudes at the suspended end of dynamically compressed riser models were obtained experimentally in a set of tests conducted at the IPT towing-tank. Those tests consisted of imposing harmonic circular motions to the top of small-scale models. Uniform current profiles were emulated by towing the models along the tank. Two different models with distinct flexural rigidities were tested, each one of them presenting a very different dynamic behavior.

Although submitted to high levels of dynamic compression, the tests conducted with the rigid model did not lead to buckling of the structure. As a result, tension amplitudes presented a steady behavior in time and out-of-plane oscillations were not observed. Tension amplitude increased monotonically with both, frequency and amplitude of top motion, in accordance with analytical studies (see, for example, Aranha and Pinto [2]).

For the more flexible model, critical compression loads were reached even at the top of the model. Buckling and out-of-plane oscillations could be visually inferred along the tests, leading to an irregular oscillation of tension amplitudes. Tension response was clearly composed by several sub-harmonics. Compared to the rigid model results, dynamic tension variation on the flexible model presented a different trend with respect to amplitude and frequency of excitation.

Dynamic tension results obtained in the towing-tank tests with the rigid and flexible riser models were compared to numerical predictions obtained with the software ORCAFLEX®.

Results have shown that the numerical approach was able to cope well with the dynamics of the rigid model, despite the influence of dynamic compression. The maximum and minimum tension values measured at the top of the rigid model were very well reproduced by the numerical model for all cases tested.

The flexible model underwent more severe levels of dynamic compression and buckling, which occurred even at the suspended end of the model for the higher amplitudes of top motion. In these cases, tests have shown that the model dynamics was essentially three-dimensional, with clear twisting of the cable. Experimental tension results have also shown the significant contribution of higher harmonics force components. Concerning flexible model results, it could be observed that discrepancies between numerical predictions and experimental results increased with the level of dynamic compression and buckling. However, it must be emphasized that the structural configuration of the model certainly contributed to such discrepancies, since the numerical model could not represent a structure with nonaxisymmetric bending stiffness.

Finally, results obtained with the rigid model were confronted with the analytical predictions of buckling loads proposed by Aranha et al. [3]. Analytical formulation was able to capture very well the buckling loads on the model and also their dependence on the frequency of excitation, confirming that the buckling loads on a catenary riser could be correctly estimated by means of a surprisingly simple analytical formulation.

Acknowledgment

This study has been conducted at the University of São Paulo, within the context of the projects TPN/CTPETRO'2000, supported by FINEP and Petrobrás and DICAS'3000, supported by Petrobrás. A.L.C.F. was supported by FAPESP, the State of São Paulo Research Foundation (98/00271-2). The authors also wish to thank Eng. Melquisedec F. dos Santos, Eng. Newton Yamamoto, and Eng. Karime H. Alves, from the University of São Paulo, for their invaluable help.

References

[1] Andrade, B. L. R., 1993, "Estudo Experimental do Comportamento Dinâmico de Linhas de Amarração," MSc thesis, Department of Naval Architecture and Ocean Engineering, Escola Politécnica, University of São Paulo, São Paulo.

[2] Aranha, J. A. P., and Pinto, M. O., 2001, "Dynamic Tension in Risers and Mooring Lines: An Algebraic Approximation for Harmonic Excitation," Appl. Ocean. Res., **23**(2), pp. 63–81.

[3] Aranha, J. A. P., Pinto, M. O., and Silva, R. M. C., 2001, "On the Dynamic Compression of Risers: An Analytic Expression for the Critical Load," Appl. Ocean. Res., **23**(2), pp. 83–91.

[4] Ramos, R., Jr., and Pesce, C. P., 2001, "A Stability Analysis of Risers Subjected to Dynamic Compression Coupled with Twisting," *Proceedings of the 20th Int. Conference on Offshore Mechanics and Arctic Eng. OMAE'01*, Rio de Janeiro, Brazil, paper OFT1042.

[5] Orcina Ltd., *Visual Orcaflex User Manual*, Orcina Ltd., Ulverston, UK.

[6] Pesce, C. P., Aranha, J. A. P., Martins, C. A., Ricardo, O. G. S., and Silva, S., 1998, "Dynamic Curvature in Catenary Risers at the Touch Down Point: An Experimental Study and the Analytical Boundary Layer Solution," Int. J. Offshore Polar Eng., **8**(4), pp. 302–310.